MASS DRIVER MODEL STUDIES OF PROPULSION AND GUIDANCE DYNAMICS

by

KEVIN SANFORD FINE

B.S., University of North Carolina at Chapel Hill

(1976)

SUBMITTED IN PARTIAL FULFILLMENT

OF THE REQUIREMENTS FOR THE

DEGREE OF MASTER OF SCIENCE

at the

MASSACHUSETTS INSTITUTE OF TECHNOLOGY

June, 1978

Signature of Author Signature redacted

Department of Aeronautics and Astronautics
May 19, 1978

Certified by Signature redacted

Thesis Supervisor

Accepted by _____

Chairman, Departmental Graduate Committee

MASS DRIVER MODEL STUDIES OF PROPULSION AND GUIDANCE DYNAMICS

by

Kevin S. Fine

Submitted to the Department of

Aeronautics and Astronautics on May 19, 1978

in partial fulfillment of the requirements for

the degree of Master of Science.

ABSTRACT

Two models have been built to study mass driver dynamics. One is a working coaxial mass driver that has been operated at accelerations of 35 gravities. The bucket is made of a coil of aluminum wire and current is supplied through contact with copper rails. Propulsion coils are discrete and operate independently, energized by photoflash capacitors and discharged by microswitches triggered by the bucket. Details of design and construction are presented along with results of operating tests. The second model uses impedance simulation to calculate interaction of levitation strips with drive and bucket coils. Profiles of guidance forces, effect of strips on drive force and calculations of drag power are presented. General considerations for track design are discussed.

Thesis Supervisor: Henry H. Kolm
Title: Senior Scientist,
Francis Bitter National
Magnet Laboratory
Lecturer, Department of
Aeronautics and Astronautics

TABLE OF CONTENTS

CHAPTER I

INTRODUCTION

A mass driver is a linear synchronous electromagnetic motor used to accelerate payloads to velocities of the order of several km/sec. Small passive carrier vehicles, called buckets, are accelerated by pulsed magnetic fields and are guided by a track using magnetic levitation forces. Studies indicate that accelerations should be 100 to 1000 earth gravities or higher. The buckets are decelerated (by generating electric power) after their payload has been released, and are returned for reuse on a return track. Mass drivers should convert electrical energy into kinetic energy of accelerated payloads at efficiencies of 75% to 95%.

Mass drivers were first proposed by Authur C. Clarke in a 1950 article.[1] The idea was later revived by G.K. O'Neill[2] and now mass drivers are being considered for two main applications in space. The first is a slingshot or pellet launcher for materials from planetary surfaces. This is not practical on the earth due to its dense atmosphere. However, for planets with little or no atmosphere, pellets from a mass driver thrown from the planet's surface can be aimed at precise points in space. The purpose in doing this is to supply raw materials to space manufacturing facilities in orbit.

A reference design for a lunar based mass driver launches 3.8 kg payloads at repetition rates of 10 per second. The lunar mass driver weighs 232 tons exclusive of power supplies and radiators, and has a yearly throughput of 600,000 tons at a launch

velocity of 2.4 km/sec.[3]

The second application of the mass driver is as a reaction engine. For this use, the mass driver is operated in orbit, and functions as a spaceship. Pellets stored onboard the ship are accelerated to high velocities to supply reaction force that propels the ship. There are two main advantages to such a propulsion scheme:

(1) Any material can be used for reaction mass. This includes waste materials such as spent space shuttle external tanks, which have been pelletized or powdered.

(2) Specific impulse can be matched to mission requirements and power plant capability for optimized performance.

For more details on mass driver applications and reference designs for both a lunar launcher and a space vehicle, consult references in Appendix A.

The work described in this paper involves two different models that have been built at the M.I.T. National Magnet Laboratory during 1977 and 1978. The first was a working demonstration model of a mass driver that was completed and first demonstrated in May of 1977. It operated as a linear synchronous motor but confinement was supplied by mechanical contact with rails instead of magnetic confinement. The model was successfully operated at accelerations of 35 gravities.

The second model was constructed during the Fall of 1977 and the Spring of 1978. It was a non-moving device that used the principles of inductance simulation to model confinement force profiles, and to calculate the effect of the levitation strips on the propulsive drive force.

Work has already begun on more advanced mass driver models. At present, a model is being constructed at Princeton University that incorporates all the major principles of a space operated mass driver. It will operate in a vacuum, use superconductors and magnetic confinement and operate at high accelerations (around 500 gravities).

CHAPTER II

BASIC COAXIAL MASS DRIVER

2.1 Introduction

The design described in this paper was created during the Fall and Winter of 1976 by Drs. Henry H. Kolm and Gerard O'Neill. Their idea was to make a device that would operate at the high accelerations (near 100 gravities) necessary for a mass driver to be used in space, but over a much shorter distance (2 m accelerating section). The model would serve to educate people on the principles of mass driver design and would also demonstrate that such accelerations could be achieved with fairly simple machinery.

In the early part of January 1977 a group of interested students began the construction work on the model. The working group ultimately included the following: Eric Drexler and Jonah Garbus, undergraduates; Bill Snow a graduate student in Aero and Astro; Bill Wheaton, a post-doctoral fellow working in space physics and myself, a graduate student in Aero and Astro. Other students helped us from time to time, principally Jon Newman from Amherst College and Mita Gupta from Bryn Mawr College. Work was done at the National Magnet Laboratory at M.I.T. under the supervision of Dr. Kolm.

The mass driver model is described in more detail in two papers by Dr. Kolm and myself published by the AIAA.[4,5]

2.2 Description of Space Mass Driver

Before describing the model, I will describe an operating mass driver to be used in space. From intensive studies during 1976 and 1977 a reference mass driver has evolved.[6] The dimensions of this design are shown in Fig. 1. All dimensions are expressed in terms of the caliber D, or mean diameter of the drive coils. The basic configuration is coaxial, with the bucket consisting of a cylinder with two superconducting coils at its ends surrounded by a line of drive coils. The strips extend lengthwise perpendicular to the coils and are arranged symmetrically around the bucket to form the track.

In present designs, the current in one drive coil goes through one sine wave of oscillation during the passage of each bucket coil. The coils are spaced by a distance ℓ_m, known as the inductance length, which is the point of maximum force (see page 40). The current in each drive coil is designed to peak when the bucket is a distance ℓ_m away, coplanar with the next drive coil. Using this system there are two phases 90° apart, which power alternate coils. A resonating capacitor is connected to all drive coils of one phase over a certain sector length.

In the vicinity of each bucket coil there are just two drive coils of one phase excited at a time. Switching silicon-controlled-rectifiers (SCR's) then connect to the sector capacitor through feeder conductors to drive coils on either side of the bucket coil. The circuit is shown in Fig. 2.

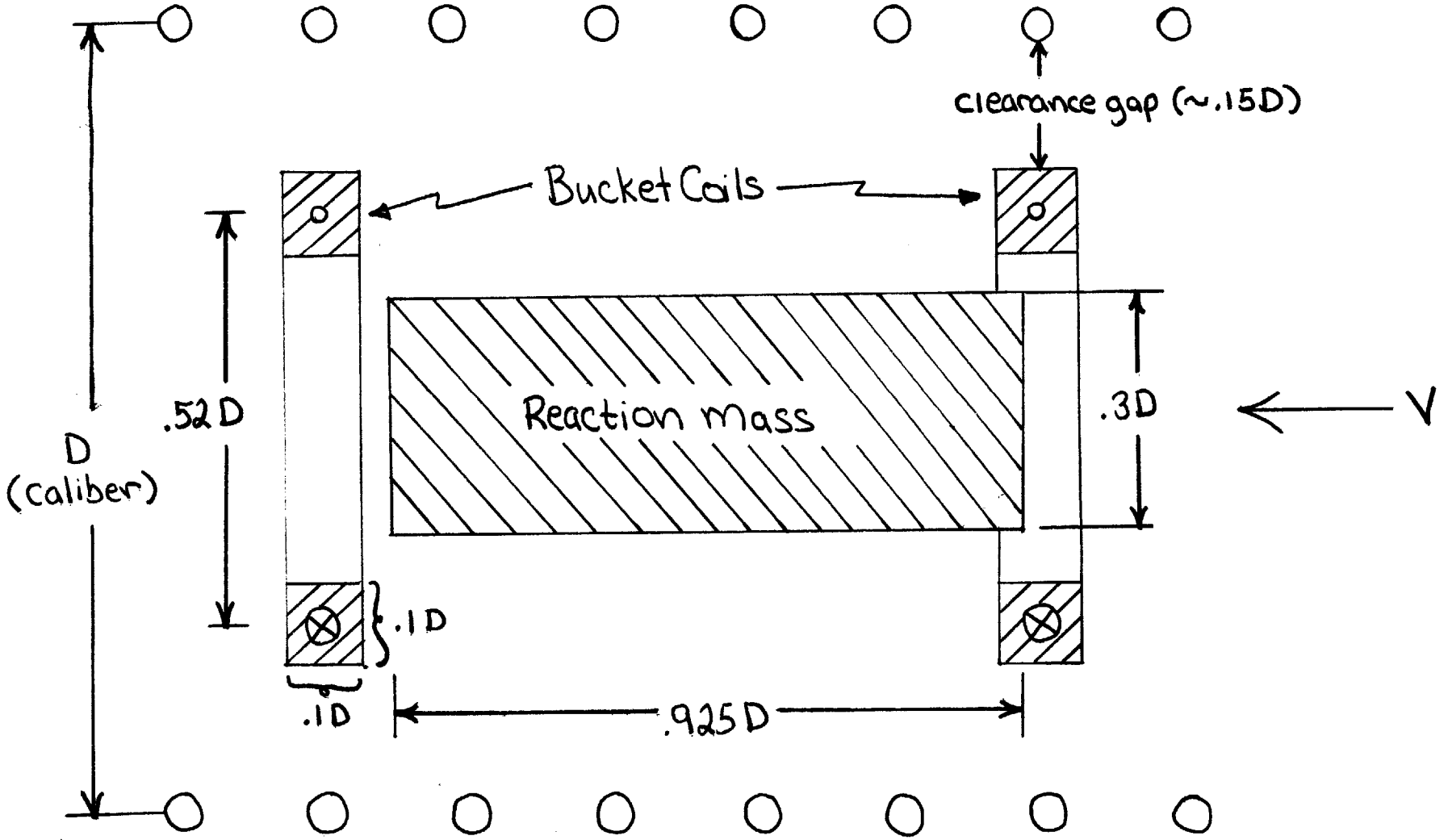

Figure 1. Cross-section of bucket and surrounding co-axial drive coils.

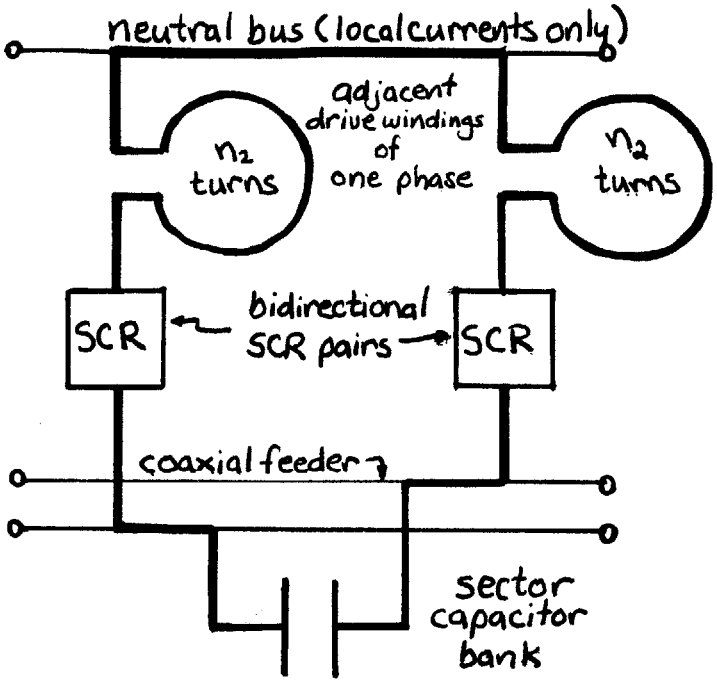

Figure 2. Sector has one capacitor bank per phase, and typically several hundred drive windings. Heavy lines show resonant circulating current. Capacitor banks are recharged from DC lines (not shown).

The mean diameter of the drive coils, referred to as the caliber D, is determined by the necessary throughput of mass. For a lunar launcher a caliber of 26 cm was chosen to supply 600,000 tons per year. The relevent design values are listed in Table 1.

TABLE 1

PARAMETERS OF LUNAR MASS LAUNCHER

Geometry:	Axial
Drive Coil Diameter:	26 cm
Peak Drive Voltage:	674 volts
Acceleration:	1000 m/s^2
Total Length (accel. and decel.):	4320 m
Bucket Mass (empty):	3.8 kg
Payload Mass:	3.8 kg
Cycle Rate (during lunar day)	0.5 → 10 Hz

Mission: Accelerate and guide lunar materials to precise point in space.

Capability: 30,000 tons/year initial, to 600,000 tons/year with added power supply.

2.3 Description of Model

The model differed from the reference mass driver designs in several ways:

(1) The model did not use superconductors. Instead, the bucket coil was constructed of aluminum wire and current was supplied through carbon brushes riding on copper rails. Also, the bucket on the model had only one coil as opposed to two in the reference designs.

(2) Confinement forces were supplied by mechanical contact with the copper rails instead of with magnetic levitation.

(3) Current through the drive coils was not a sine wave but instead was a pulse of current in one direction. Thus, the drive coils only pushed the bucket, while in the actual device they would both push and pull.

(4) The bucket was braked with friction. In an actual mass driver braking would involve no mechanical contact and would be used to generate power.

The dimensions of the model are shown in Fig. 3. The caliber was chosen as a compromise between the expense of large size and the precision needed for small size.

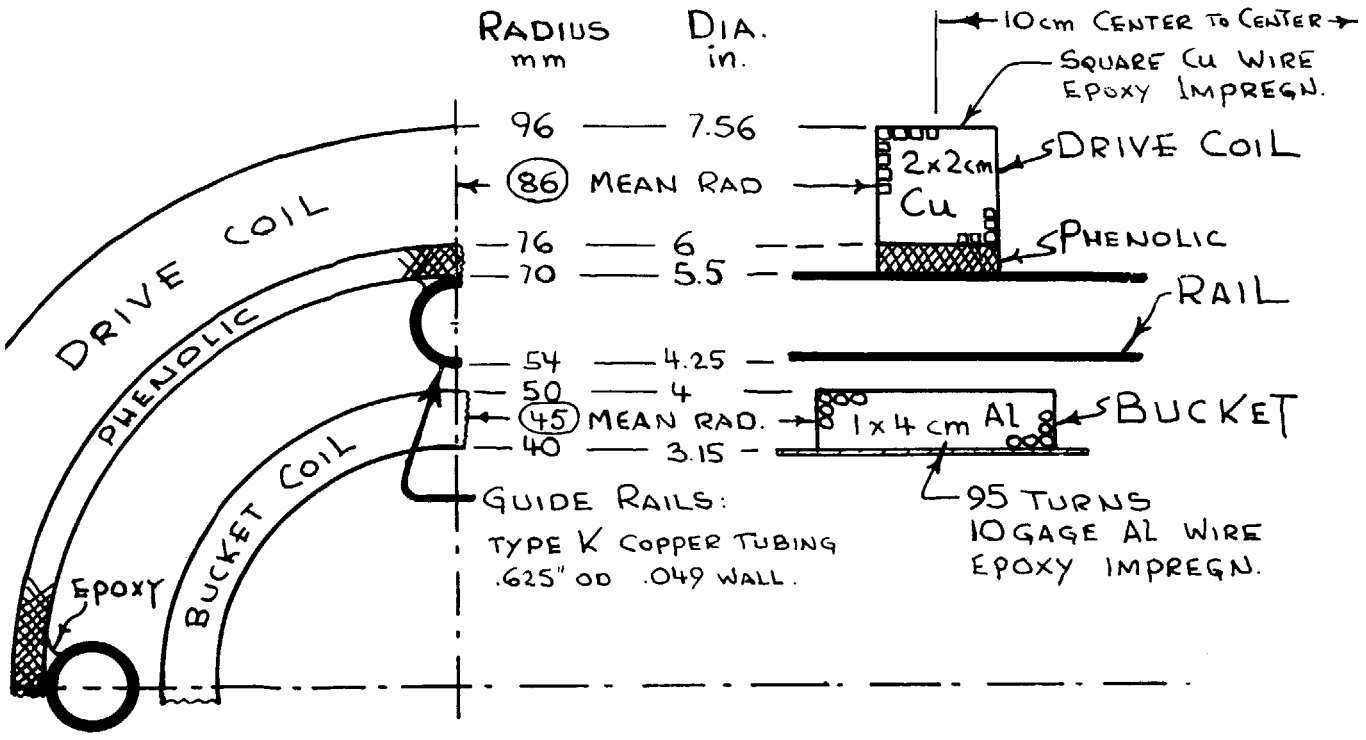

Figure 3. Dimensions of the basic four-inch caliber coaxial mass driver (Drawing from Ref. 4).

The accelerating section consisted of 20 drive coils spaced 10 cm apart center to center. The coils were mounted on top of an eight foot aluminum I-beam. Electronics were attached to the webbing of the I-beam.

The bucket rode on four copper K type 1.27 cm (1/2 in.) plumbing tubes. To supply current to the bucket, four 12 volt automobile batteries were connected in series to the pipes through a relay which was connected to the firing switch. A diagram of the bucket is shown in Fig. 4. The brushes were held onto the pipes by the beryllium-copper strips, which also provided a conducting path to the aluminum coil. Design values of the bucket

TABLE 2

MODEL BUCKET COIL DESIGN VALUES

Coil:	95 turns of gauge 10 aluminum wire
Bucket Mass:	1/2 kg
Inductance:	789 μH
Resistance (at 20°C):	.18 μ

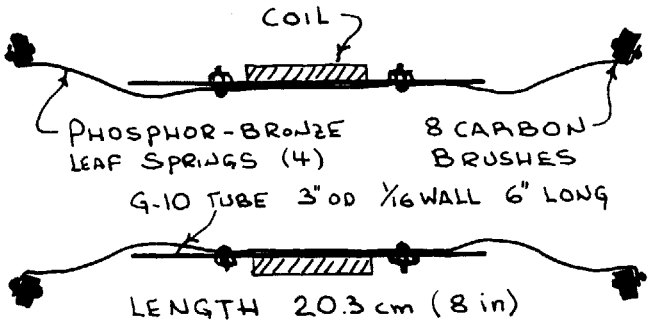

Figure 4. Section view of half-kilogram bucket (Drawing from Ref. 4).

are summarized in Table 2. Note that at the resistance value given, with 48 volts across the bucket, a current at 270 amps would flow.

The basic drive coil circuit and its waveform is shown in Fig. 5. Since the capacitors used were electrolytic, a crowbar diode was included to protect them from voltage reversal. The capacitors are 450 V, 1800 MFD, and the total energy stored in each capacitor when fully charged is 182 J. The peak current reached upon discharge of each coil depends upon the number of turns in the coil. These values are listed in Table 3.

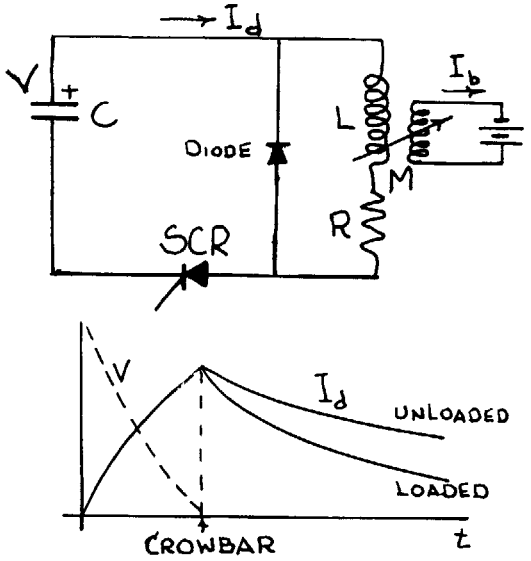

Figure 5. Basic propulsion circuit and waveforms (Drawing from Ref. 4).

TABLE 3

DRIVE COIL PARAMETERS

COIL NUMBER	TURNS	WIDTH	BUILD	MAXIMUM CURRENT
1	80	6 cm	2 cm	500 A
2	64	5	2	625
3	64	5	2	625
4-10	32	2	2	1.25 kA
11-20	16	2	2	2.5

2.4 Design Logic

The acceleration of the model was chosen as 100 gravities to match performance characteristics of existing reference designs. Then, after the caliber was chosen, the model was designed on the basis of greatest efficiency for the least cost and greatest simplicity.

The discharge waveform of a drive coil is shown in Fig. 5. A change in the number of turns in a coil had two effects upon this waveform. Peak current goes inversely as the number of turns. Since SCR cost increases with current rating, it is thus desirable to use as many turns as possible. This, however, increases rise time, since rise time goes as

$$LC = n^2 L_o C \qquad (2.1)$$

It is desirable for optimum propulsion for the current peak in the drive coil to occur no later than the time when the bucket is at its maximum thrust position (about 3.5 cm from the drive coil). These two constraints led to the optimum number of turns listed in Table 3.

The decay constant of the curve in Fig. 5 is L/R which is independent of the number of turns in a drive coil and proportional to the cross-sectional area. Current in a drive coil should not

die while it can still accelerate the bucket. This resulted in a larger cross-section for the first three coils where the bucket was moving slowly. Coil cross-sections are listed in Table 3.

In order to calculate average acceleration, Grover's book on inductance calculations was used. Differential equations of motion were solved numerically using programmable pocket calculators. For listings of these programs and a more in depth discussion of design logic refer to Kolm's paper.[4]

2.5 Construction of Model

The first parts made were the drive coils. It turns out that for reasons of economy the number of turns in the coils should be varied down the length of the track. We did this by making coils of 8 layers of 8 parallel square (.32 cm or 1/8 in.) copper wires and then connecting the wires together in 2 different ways; one to make 16 turn coils and the other way to make 32 turn coils. If the coil at the beginning of the accelerating section is number 1, then coils 4-10 are 32 turn and 11-20 are 16 turn.

To make the coils, we first cut a mandrel out of .64 cm (1/4 in.) wall, 13.97 cm (5 1/2 in.) inner diameter paper phenolic tubing. To attach the wires to this mandrel we drilled 8 holes into the mandrel in a V-shaped pattern through which we inserted the square wires. We then clamped wood sides onto the mandrel one of which had a metal disk attached that could be held in a lathe chuck on a coil winding machine.

While the machine was winding the coil we spread a thick layer of epoxy onto the wires. After the coil was wound, we clamped it, cut the wires and removed it from the chuck and placed it into an oven to cure the epoxy. After hardening the wood sides were removed (they had been covered with mylar to keep them from gluing to the coil) and all that remained to be done was to make the external connections. We found we could make 1 coil in 2 hours using this method.

The first 3 coils were made with a bigger cross-section. We wound these with a single strand of .64 cm by .32 cm (1/4 in. by 1/8 in.) rectangular copper wire.

To mount the coils, we first made spacers to which we clamped the copper pipes. Then we slid the coils onto the pipes and bonded them with epoxy. We had several problems with this method, mainly arising from the fact that our coils were slightly undersize on the i.d.

Figure 6 illustrates the method we used to mount the structure of coils and pipes to the I-beam. We cut pieces of aluminum U-channel that were a little wider than the coils, and attached them to one of the flanges of the I-beam, so they provided cradles for all the coils. Then we cut phenolic strips and attached these to the sides of the channels, so that each coil sat in a little bathtub-like structure. After alignment with little wedges and shims cut from scrop material we filled the tubs with a mixture of sawdust and epoxy. After the epoxy hardened the coils were

mounted and well aligned.

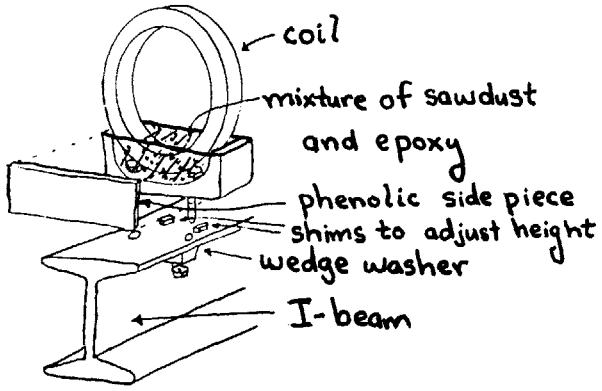

Figure 6. Disassembled view of coil mounting.

The I-beam also provided space for the electronic to be attached. Figure 7 is a photograph of the accelerating section from the side. Note that the long dimension of the I-beam cross-section is vertical, with the coils attached to the top flange. The capacitors, which are the two cans sitting in the I-beam in the photograph, are small enough to fit against the 8-inch web of the I-beam, attached with aluminum straps. The holes shown in the web of the I-beam are where the SCR's and diodes are to be mounted. An unmounted SCR is shown to the right of one

of the capacitors in the photograph.

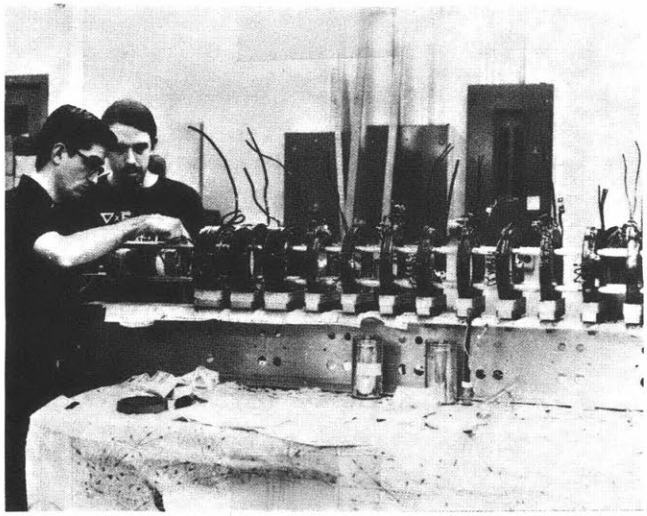

Figure 7. Photograph of the accelerating section from the side. The workers are Bill Snow (L) and Eric Drexler. Two capacitors and an SCR can be seen in the middle of the I-beam.

The bucket was made with G-10 tubing. The bucket coil was mounted onto the mid-section of the tube by first clamping phenolic rings onto the tube with hose clamps and using this as a form to wind wire onto the tube on a lathe. Epoxy was added to bond the wire together. The wire used was 10-gauge aluminum wire which was soft and wound easily.

The final component to the accelerating section was the microswitches. It was determined that the best point to discharge the capacitors was when the bucket was 1 cm before being

centered in the drive coil. The mounting of the switches and backet acutator arm is illustrated in Fig. 8.

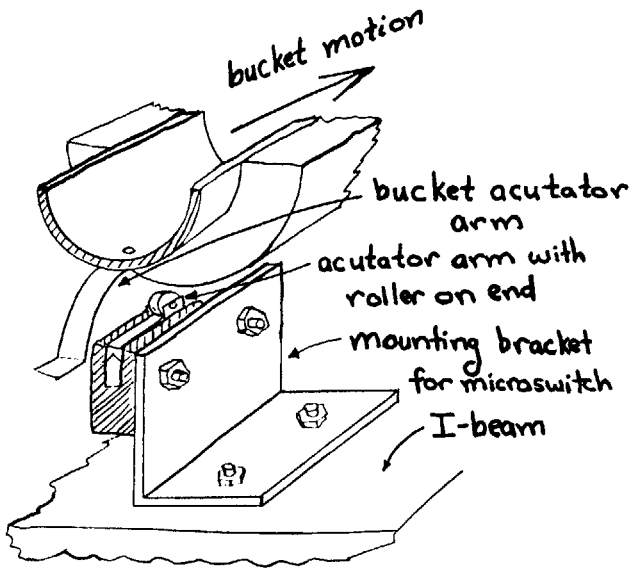

Figure 8. Microswitch on its mounting.

2.6 Tests with Model

With four 12 volt batteries connected in series to the bucket circuit, average accelerations were measured between 20 to 25 gravities. Calculations were in good agreement, since they predicted 25 gravities. One test was conducted to reach the full 100 gravities of acceleration. The bucket coil was immersed in liquid nitrogen to lower its resistance to one-tenth room temperature resistance. The bucket derailed twice before finally firing, and acceleration was measured at only 35 gravities.

This was certainly partially due to warming of the bucket during the derailed attempts. A firing with a cooled bucket was not tried again.

The model was regularly demonstrated with six 12 volt auto-batteries, which regularly gave accelerations of 25 gravities. During the firings an average of two capacitors would not discharge. This was due to the crudeness of the microswitch triggering method. Another problem encountered was damage to the microswitches by the actuator arm of the bucket. An attempt was made to replace the microswitches with optical switches, but due to limitations in time, money and expertise this was abandoned.

CHAPTER III

EXPERIMENTS WITH IMPEDANCE MODELS

3.1 Introduction

This section describes some experiments made with impedance models at M.I.T. during the Fall of '77 and the Spring of '78. The models were built in order to determine the effect of the electrical interaction of the guidance strips with the drive and bucket coils. Calculations were made of guidance force profiles with different tracks, of drag on the bucket, and of the shielding effect of the strips on the bucket drive coil forces.

The models were simply and cheaply constructed, made of plywood, wire and strips of aluminum. They were static and only steady-state forces were measured. The experiments consisted of measurements of the changes in inductance and resistance as the positions of coils of wire were changed. The theory that led from these measurements to the above calculations is called the theory of impedance simulation. It was developed extensively in the late sixties and early seventies in order to analyse magnetic levitation schemes for high speed trains. The present paper relies heavily on this work.

Since the results from these measurements may be used in future studies, I have tried to present them simply and with as

much generality as possible. It is my hope that they can be understood with minimum effort.

3.2 Theory of Impedance Simulation

Impedance simulation relates measurements made with a stationary coil with AC current to forces on a moving DC coil. The basis premise is that the eddy currents produced by both coils will be geometrically similar. The reasoning behind this goes as follows: Imagine that we have a coil of wire with DC current moving parallel to a strip of conductor. Along the strip, eddy currents will be induced by the change in the component of magnetic field perpendicular to the strip (B normal). At any particular instant, this component varies at the

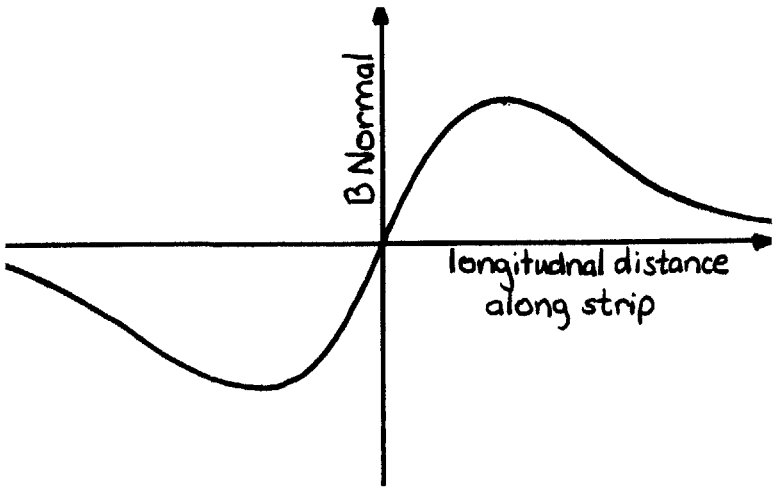

Figure 9. Normal field variation along guidance strip.

strip's surface as shown, where the abscissa is distance along the strip. This curve can be approximated by a sine wave of the appropriate wavelength. If we imagine that we have such a sine wave of wavelength λ, then if the DC coil is moving with a speed v, then B normal will vary as $\sin \frac{2\pi vt}{\lambda}$ when the coil passes a fixed point. B normal will also vary in exactly the same way if the coil is stationary and the current varies as a sine wave with frequency v/λ. This means that both coils will induce geometrically similar eddy currents.

If we vary the frequency of the signal in the stationary coil, it is equivalent to varying the velocity of the DC coil as $v = f\lambda$. Remember that λ is fixed by the geometry of the coil and track.

Note that this correspondence is correct only to the degree to which the sine wave approximates B normal. It becomes better, however, as velocity (and f) increase. This is due to the fact that the distribution of the eddy currents approaches asymptotically a high speed limit because the difference between eddy currents produced at different high frequencies will approach zero. Now imagine that we represent the B normal curve by all its Fourier components, adding the ones beyond the lowest order component. If the frequency of the lowest order component is high enough, then the higher frequency Fourier components will

not differ significantly in their effect. Thus the eddy current correspondence becomes exact as f approaches infinity.

The DC coil corresponds to a bucket coil moving down a track made of conducting strips. If we build a model of a mass driver with a coil of wire and strips of metal, we can measure how the inductance of a geometrically similar AC coil changes as a function of position. Since the eddy current pattern is geometrically similar to that of the moving bucket, we can deduce the guidance force profile on a moving bucket from these measurements. At any moment the electrical energy stored in the bucket-track system is given by

$$E = \frac{1}{2} L_b I^2 \tag{3.1}$$

where I = current in the bucket and L_b = inductance of the bucket. From the above discussion we can relate L_b to the measured inductance of the AC coil by

$$L = \frac{n}{N} L_b \tag{3.2}$$

where n = number of turns in the AC coil and N = number of turns in the bucket. Since the bucket is superconducting I will vary so as to keep a constant flux. Thus,

$$\phi = \frac{n}{N} LI = \frac{n}{N} L_o I_o \tag{3.3}$$

where the subscripts indicate an initial condition.

Force can be calculated from the gradient of energy, so that

$$F = -\nabla E = -\frac{1}{2}\left(\frac{L_o}{L}\right)^2\left(\frac{N}{n}\right)^2 \nabla L\ I_o^{\,2} \tag{3.4}$$

If the model coil has dimensions that differ from the bucket by some scale factor, the inductance will be proportional to that scale factor. Thus ∇L will be independent of the scale factor. This means that $F/I_o^{\,2}$ versus a normalized displacement variable will be the same for, all geometrically similar mass drivers. This is the basis for normalizing all the plots in this paper.

It is also possible to determine drag force profiles using measurements of changes in the AC resistance of the model coil as it is moved inside the track. The power dissipated due to eddy currents in the strips in the impedance model is

$$\frac{1}{2}\, i_p^{\,2}\left(R - R_o\right) \tag{3.5}$$

where i_p = peak current in the AC coil, R = resistance of the AC coil in the track, R_o = resistance of the AC coil outside of the track. Due to the geometric similarity of the eddy currents this will be equal to the drag power on the bucket if the current in the bucket is i_p. Relating the current in the

bucket, I, to its initial value I_o by $I_o = \frac{L}{L_o} I$ we have

$$\left(\frac{vF_d}{I_o^2}\right) = \frac{1}{2}\left(\frac{L_o}{L}\right)^2 \left(R - R_o\right)\left(\frac{N}{n}\right)^2 \tag{3.6}$$

This expression is also independent of the scale factor.

Another important effect of guide strips is to produce eddy currents which oppose the action of the drive coils. The strips act as a shield between the drive and bucket coils. The strips become more opaque to the drive coil fields, as frequencies of the drive coil currents become higher.

The force between the drive and bucket coils is given by

$$F = -I_b i_d \frac{dM}{dx} \tag{3.7}$$

where M = mutual inductance between drive and bucket coils, x = separation of drive and bucket current, i_d = drive coil current. M can be measured as a function of bucket-drive coil position with the impedance model, and from this we can determine the effect of the strips on the drive force.

The effect of varying strip width can be understood with the following simple model. Imagine that we have two sheets of conductor, one which is whole and the other which is divided into n pieces. If we model each piece as a current loop, then

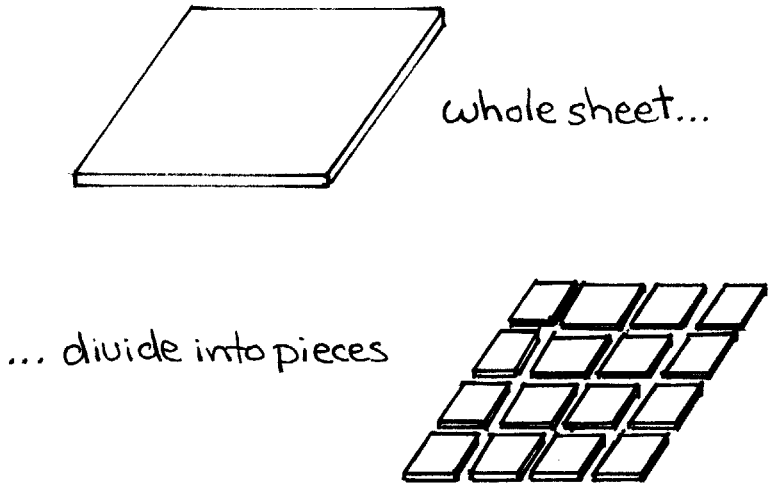

Figure 10. Conducting sheet divided into pieces.

$$\text{resistance of small loop} = \frac{\text{resistance of large loop}}{\sqrt{n}} \tag{3.8}$$

If we immerse both sheets in the same time varying fields, then the magnitude of the eddy currents will be given by the ratio of induced voltage to resistance. Induced voltage will go as the area of each piece, or n, so that

$$\text{current induced in small loop} = \frac{\text{current induced in large loop}}{\sqrt{n}} \tag{3.9}$$

Thus eddy currents will be smaller when the conductor is divided into more pieces, given the same amount of conductor. This suggests that all the phenomena associated with the eddy currents

(i.e., drag, lift forces and reduction of dM/dx will be less pronounced when the track is divided into more strips.

This theory assumes that dividing a guideway strip into n narrower strips is equivalent to dividing a square into n smaller squares. This is true only if the eddy current distribution remains geometrically similar, i.e., that the area to perimeter ratio (or voltage to resistance ratio) of eddy current elements remains constant. This assumption is only approximately true.

3.3 Experimental Apparatus

The geometry of a coaxial mass driver is shown in Fig. 11. The track is composed of curved aluminum strips that surround the superconducting bucket. The bucket is shown here with two coils but more may be used in practice. Note that there is no contact between any of the moving parts, which is necessary because of the extremely high speeds.

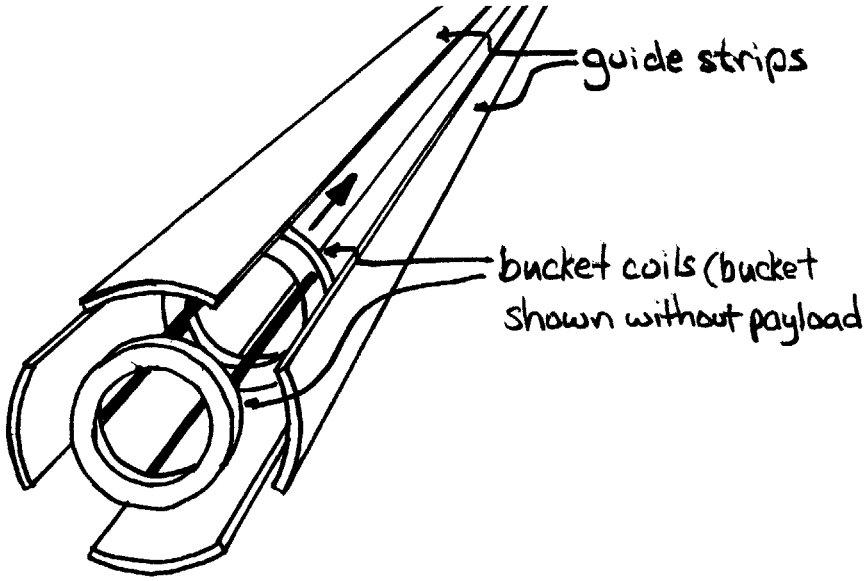

Figure 11. Geometry of coaxial mass driver.

The impedance model consisted of only one coil which was made of 10 gauge aluminum wire, wound onto a plywood coil form and impregnated with epoxy. The bucket coil was held by a phenolic tube that went through the center of the coil and was supported at its ends by threaded rods which were used to position the coil. The track was made from rectangles of ALCOA alloy 1100 aluminum, bent into arcs that fit onto plywood rings of radius 10 cm. Three tracks were made, with 3, 6 and 12 strips each. Each set of strips was designed so that they covered 50% of the surface surrounding the rings, so that each track contained the same amount of aluminum.

A drive coil was made from the same aluminum wire used to make the bucket coil. It was made simply by winding the wire around a section of the track and using masking tape to bond it together. When finished it proved to be slightly oversized so that it fit easily onto the outside of the track. A scale was made from graph paper and pasted to the outside of the track so that the relative position of the drive and bucket coils could be measured.

Dimensions of the model are summarized in Table 4. The dimensions were chosen as close to the reference design created at the 1977 Ames summer study.

The measurements of impedance were made with two different meters, both manufactured by General Radio. The first one used was a 1657 RLC Digibridge, which gave four digit accuracy but

was limited by the fact that it was restricted to only two frequencies, 220 and 1000 Hz, both of which are too small to measure the high frequency limits of impedances in the model. For this reason, another instrument was also used, an older model impedance bridge, the General Radio 1650-A. The measurement frequency was supplied by an external oscillator, so that frequencies above 1 KHz could be reached.

A photograph of the experimental set up is shown in Fig. 12. Note that the track and the end supports were attached to a plywood base. The impedance bridge is shown at the left, with its external oscillator to the right. The drive coil is leaning against the track. Not shown are micrometers attached to supports at each end of the bucket coil tube. These measured the changes in position of the coil.

Figure 12. Photo of the impedance simulation model.

TABLE 4

DIMENSIONS OF IMPEDANCE MODELS

BUCKET COIL

Cross-Section:	2 cm build by 1.91 cm width
Mean Radius:	5.3 cm
Number of Turns:	54 turns of 10 gauge aluminum wire

DRIVE COIL

Cross-Section:	2.54 cm build by 1.91 cm width
Mean Radius:	10.6 cm
Number of Turns:	36 turns of 10 gauge aluminum wire

TRACKS

3 tracks; 3, 6 and 12 strips. All covered 50% of surface area with aluminum. Aluminum used was .32 cm (1/8 in.) thick ALCOA alloy 1100.

Inside radius of curvature of strips = 10 cm

3.4 Guidance Force Profiles

There is an approximate method of calculating the high speed guidance forces that can be used as a check on the experimental measurements. It represents the upper limit of guidance forces. It was presented in the final report of the Ames '77 summer study.[6]

The calculation models the bucket as an octagonal current loop (see Fig. 13). The guidance strips surround the loop, and their effect is modeled as image currents in the shape of an octagon. The image currents are the same distance, call it s, away from the strips as the nearest segment of the bucket octagon. We assume that the force on each element of the bucket coil is caused only by its mirror image in the nearest guideway surface.

The Lorentz force per unit length on each circuit element is given by

$$F = IB = \frac{\mu_o I^2}{4\pi s} = I^2 \left(\frac{1}{s}\right) \times 10^{-7} \text{ newtons/meter} \qquad (3.10)$$

Call R = radius of the guideway and r = radius of the bucket coil. Then the length of each current element in the bucket is

$$\ell = 2(\sqrt{2} - 1)\, r \qquad (3.11)$$

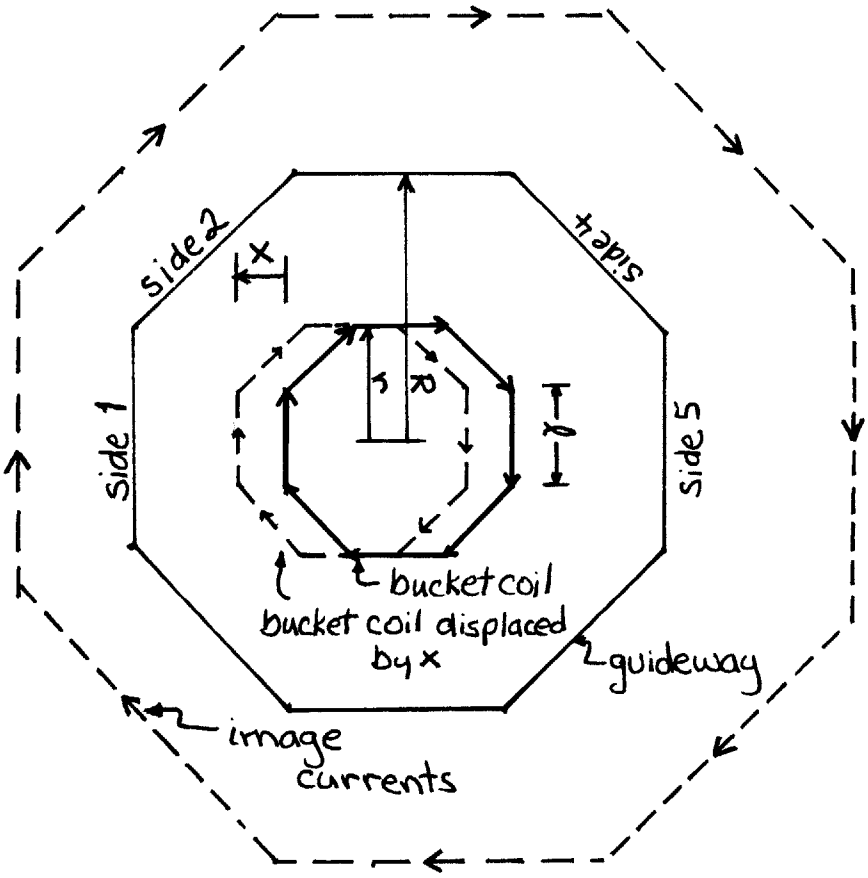

Figure 13. Geometry of the octagonal approximation.

If the bucket is displaced a distance x to the left (dashed) line), the images move accordingly and s is different for each element.

$$S_1 = (R - r)\left(1 - \frac{x}{R - r}\right) \tag{3.12}$$

$$S_5 = (R - r)\left(1 + \frac{x}{R - r}\right) \tag{3.13}$$

$$S_2 = (R - r)\left(1 - \frac{x}{\sqrt{2}\ (R - r)}\right) \tag{3.14}$$

$$S_4 = (R - r)\left(1 + \frac{x}{\sqrt{2}\ (R - r)}\right) \tag{3.15}$$

Total force is then given by

$$F = F_1 - F_5 + 2F_2 - 2F_4 \tag{3.16}$$

This force depends upon the factor r/R, which for all impedance models was chosen equal to 0.53. The value was chosen because of its use in previous studies.[6]

This model assumes total envelopment of the bucket by the track. All my impedance models were only half enveloped. Thus, in this calculation, we multiply the forces by a factor of 1/2.

There are several approximations in this model. Forces due only to close current elements are included. Wires with thickness are modeled as filaments. The force law used is that

between infinite straight wires and the edge effects of finite strip width are ignored. All of the approximations tend to make the force values in the calculation larger than in an actual mass driver. The main value of the calculation is to give us an upper bound and to indicate the order of magnitude of the forces. The results of the octagonal approximation are shown in Fig. 14.

The results of the experiments with the impedance models is presented in Figs. 15 through 18. These measurements were all made at a frequency of 20 KHz. In order to relate this to a velocity of a moving bucket, we introduce the concept of inductance length. Imagine a drive and bucket coil, both with constant current, with the bucket moving through the center of the drive coil. The inductance length is that distance from the drive coil at which the bucket coil experiences maximum thrust. It corresponds to one quarter of the wavelength of the sine wave that approximates the magnetic field of the bucket (see section on theory). For the diameter ratios used in the impedance model, this distance, labeled ℓ_m, is given by $\ell_m = (.75)\ r$, where r = radius of the bucket. Once we know the wavelength, speed can be calculated from $v = f\lambda$. For f = 20 Khz and r = 5.3 cm, v = 3180 m/sec. Even more important is the skin depth at this frequency in relation to the thickness of the strips. Skin depth in aluminum at 20 KHz is .06 cm. This is about one-fifth the thickness of the guide strips used in the model (1/8 in.).

When the thickness of the strips is larger than the skin depth, the strips keep most of the electromagnetic wave from

penetrating through them. This explains the variations of guidance forces with speed. At low speeds, less magnetic field penetrates the strips as speed increases, so lift forces also increase. Once the skin depth becomes significantly less than the strip thickness, increasing speed simply acts to crowd eddy currents closer to the strip surface, without increasing their magnitude. This accounts for the fact that guidance forces approach an asymptotic limit. The 20 KHz frequency used in the impedance models was chosen because it was the highest practical frequency at which to make measurements, and has a small enough skin depth to give the high speed limit of the guidance forces.

Experiments were conducted to determine the angular dependence of the guidance forces (Figs. 15 through 17). As can be expected intuitively, the 3 strip track strongly showed angular dependence while the 12 strip track showed almost none. From arguments given in Section 3.2, it can also be expected that guidance forces will be greater with fewer strips. At maximum deflection of the bucket, averaging over the different values at the different angles, we see that guidance force in the 6 strip track is 16% less than in the 3 strip, and that it is about 38% less in the 12 strip versus the 3 strip track. Thus our theory is confirmed by measurements. Also note that guidance force values are about one-third as large as the octagonal calculation, which is reasonable considering the approximations

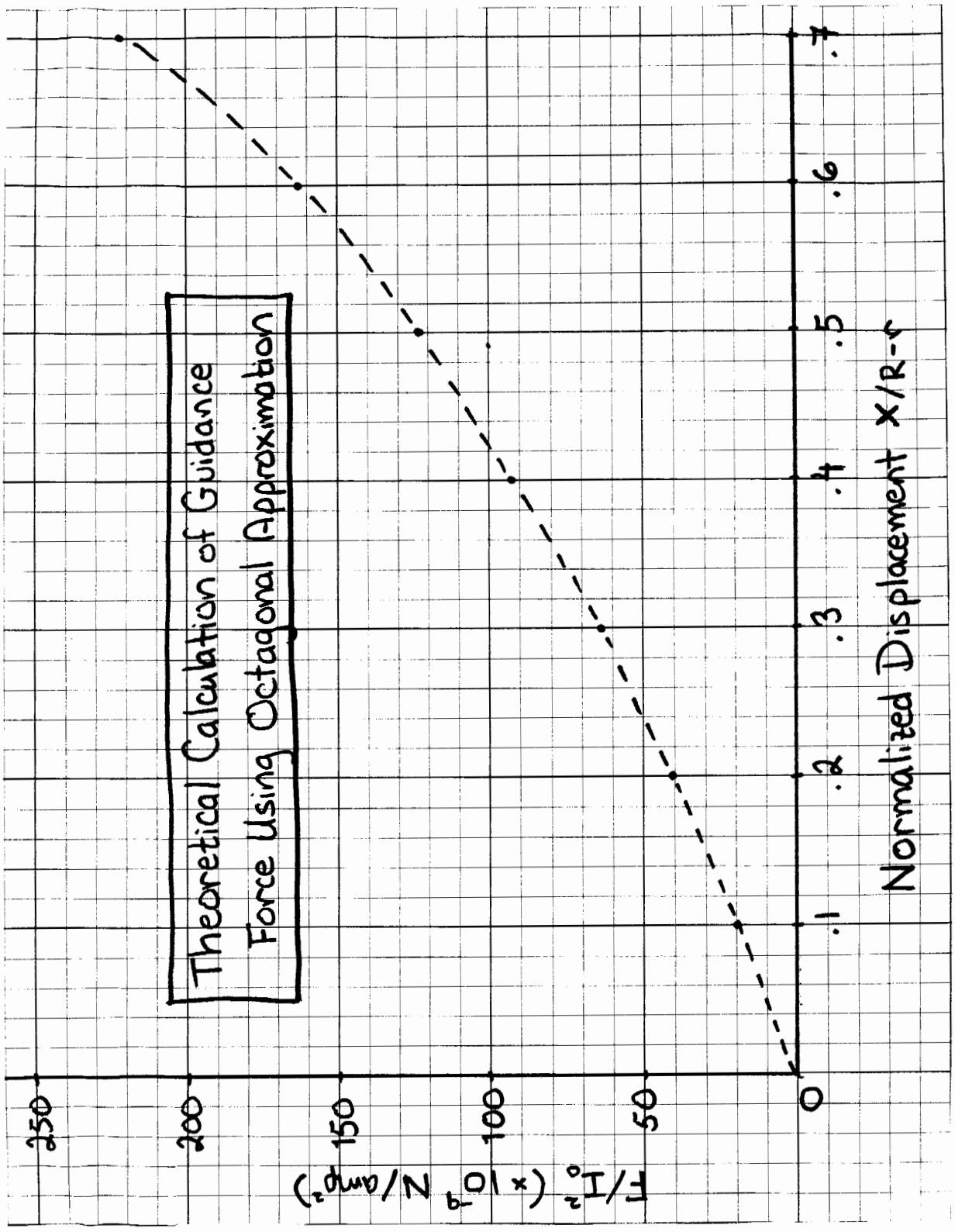

Figure 14. Results of the octagonal approximation calculation.

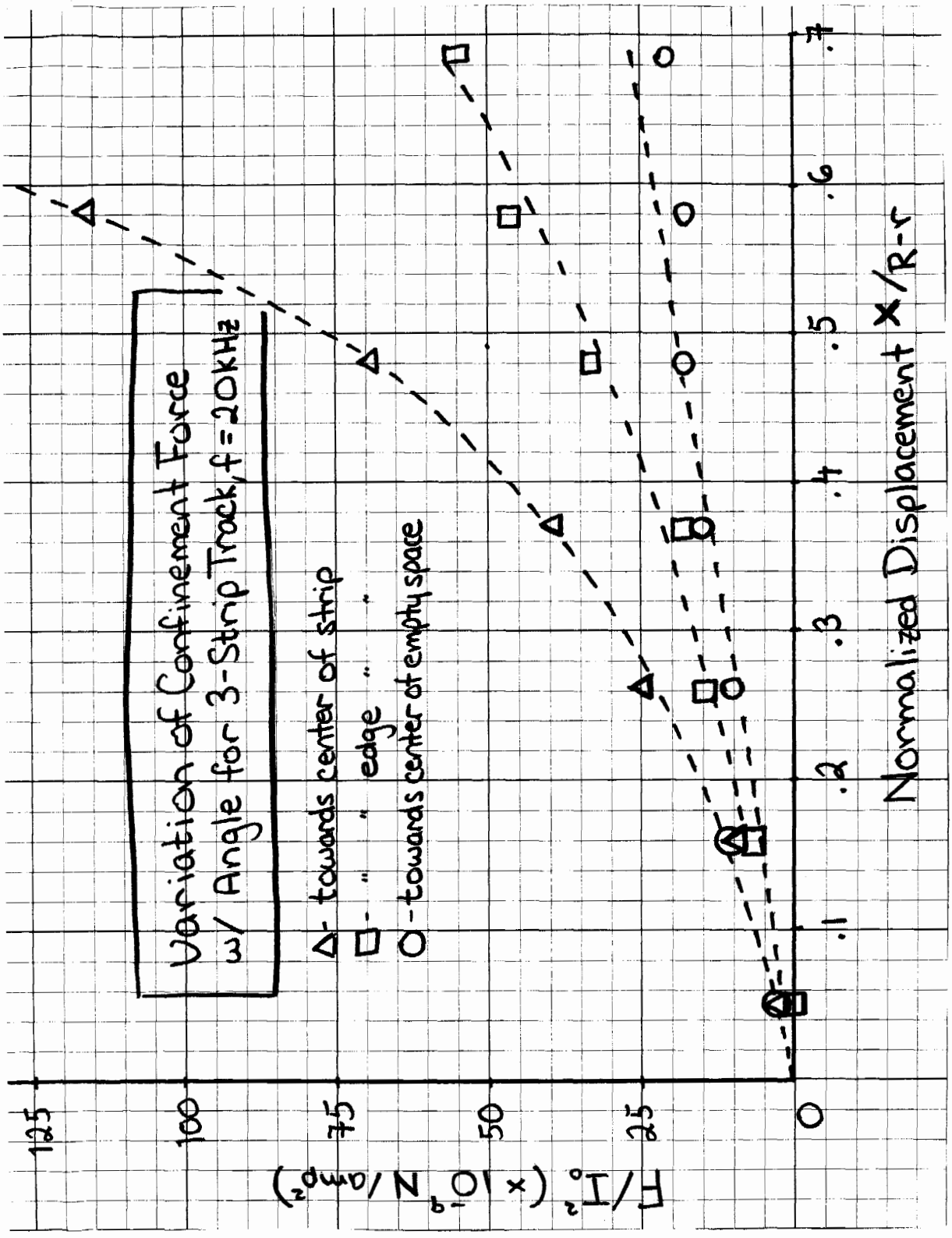

Figure 15. Measured variation of confinement force for 3-strip track as a function of angle.

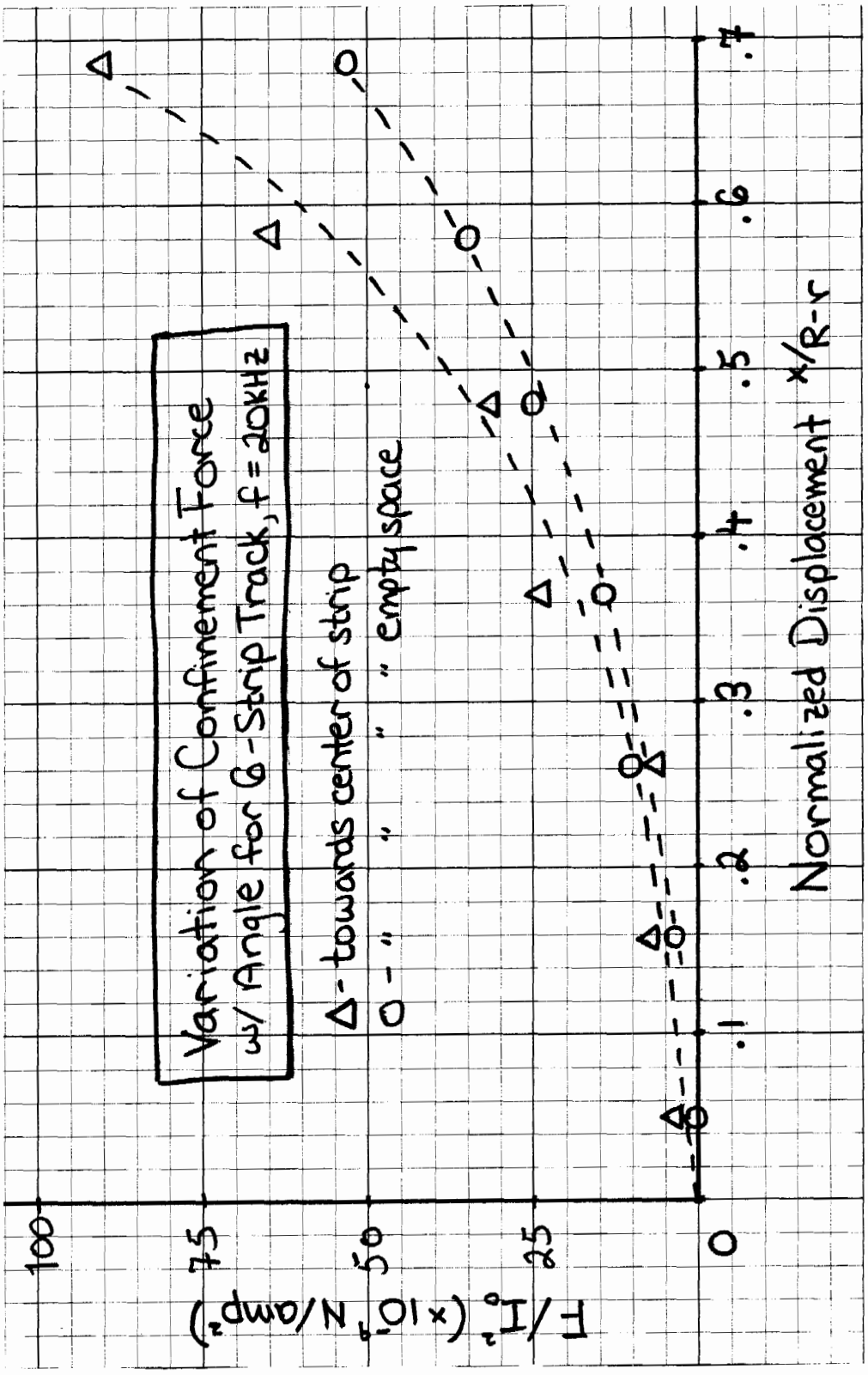

Figure 16. Measured variation of confinement force for 6-strip track as a function of angle.

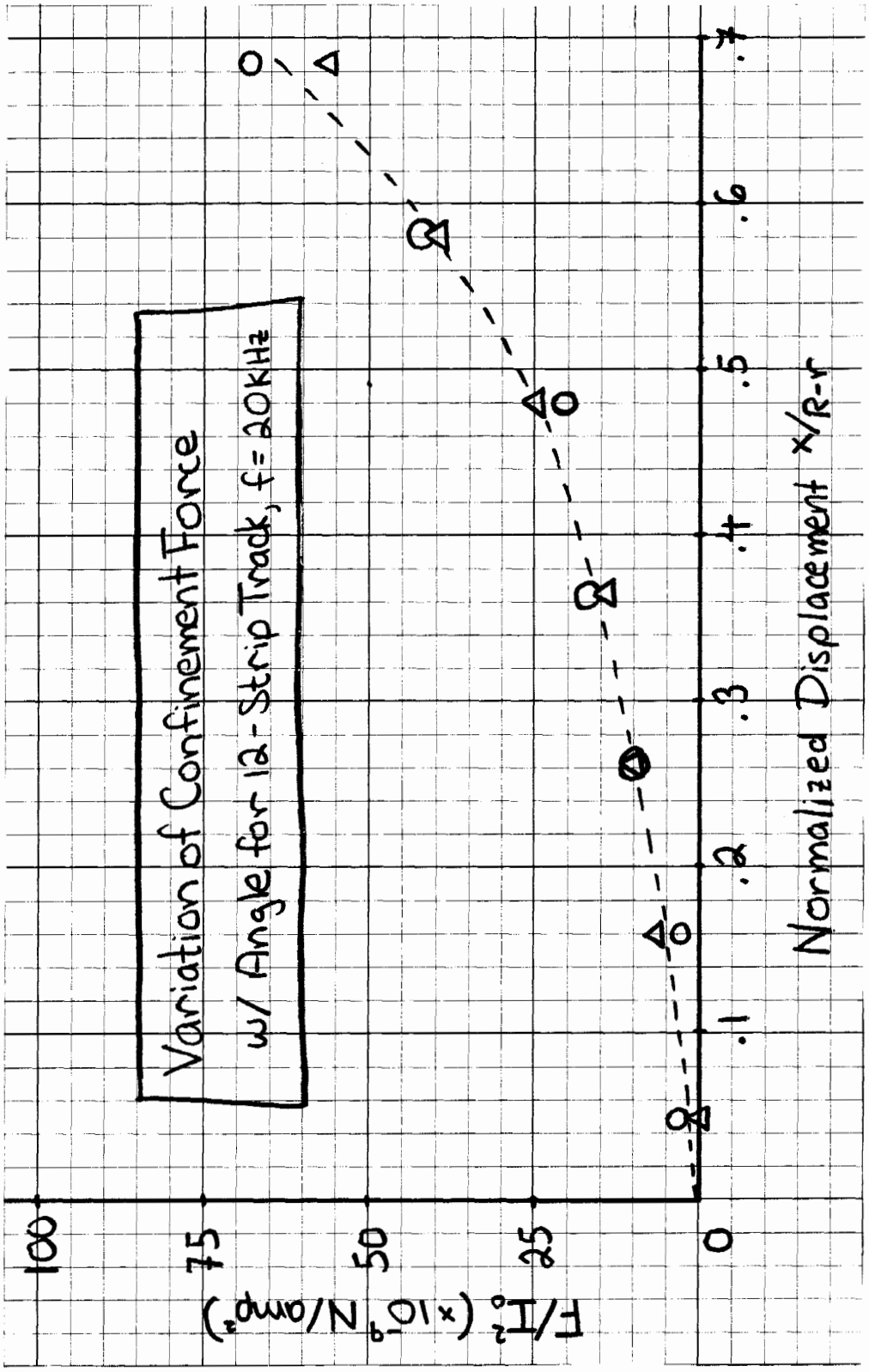

Figure 17. Measured variation of confinement force for 12-strip track as a function of angle.

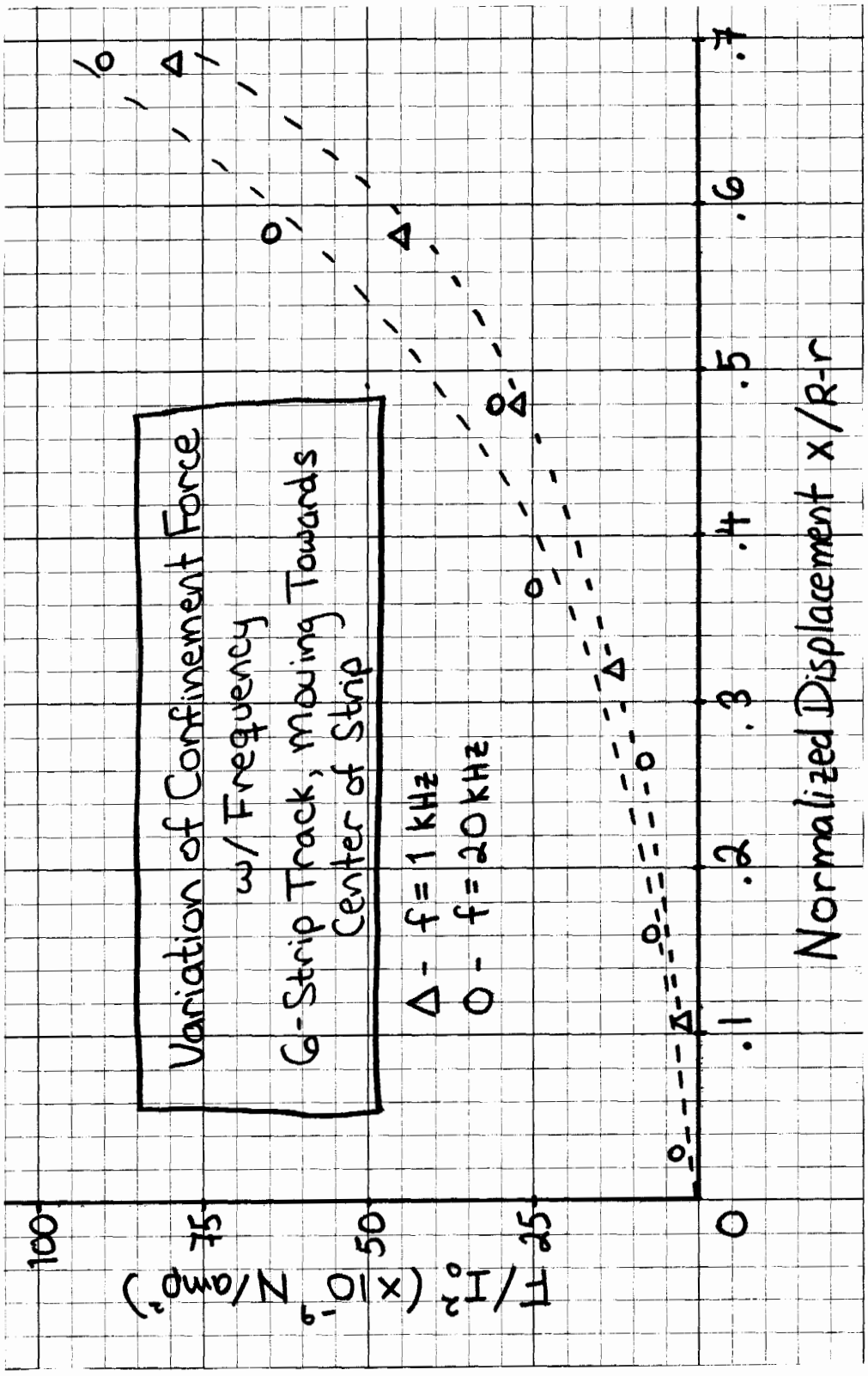

Figure 18. Measured variation of confinement force at two different frequencies with 6-strip tracks.

made in the calculation.

Attempts were also made to measure the guidance force profiles at frequencies lower than 20 KHz, so that their variation with speed could be calculated. However, because of difficulties with the impedance bridge, values could be obtained at only one frequency, 1 KHz. This frequency corresponds to a speed of 159 m/sec. and a skin depth 0.85 times the thickness of the strips. The results are graphed in Fig. 18. It can be seen that there is a difference of almost 20% in the guidance force at the two frequencies.

3.5 Effect of Strips on Drive Force

The drive coil fields produce eddy currents in the guidance strips that reduce the drive force. This effect shows itself as a reduction in the space gradient of mutual inductance, ∇M, between the drive and bucket coils. This reduction was measured with the impedance models by measuring mutual inductance as a function of drive coil position with various tracks.

A theoretical calculation of dM/dx is shown in Fig. 19. It was made from values found in a book by Grover,[9] and serves as a check on our experimental measurements.

The results of impedance model experiments are shown in Fig. 20. They agree well with the theoretical curve in Fig. 19. While the results show a good deal of experimental fluctuation, it is still clear that the eddy current effect is greatest in

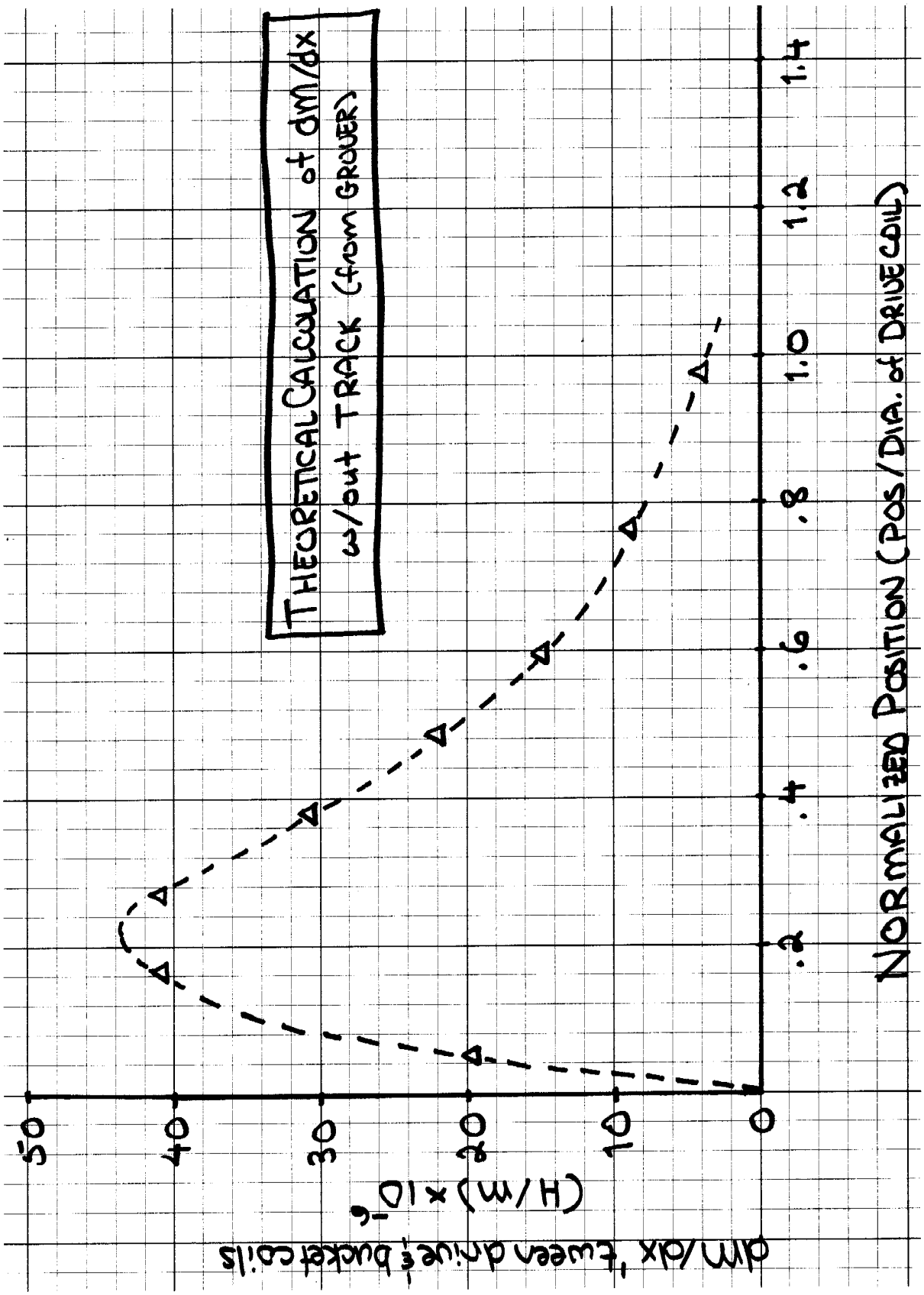

Figure 19. Theoretical calculation of mutual inductance gradient between drive and bucket coils.

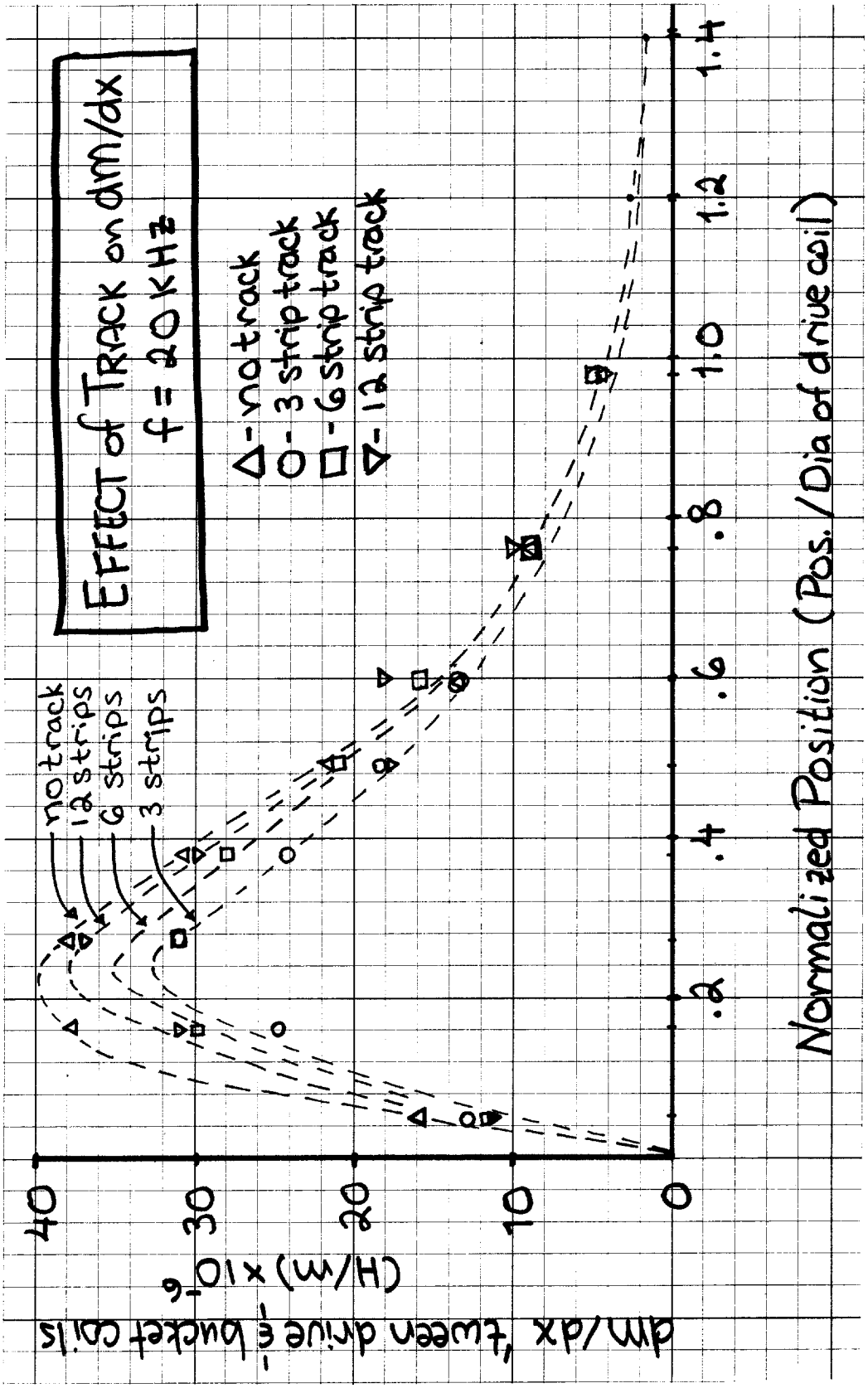

Figure 20. Experimental measurements of mutual inductance gradient between drive and bucket coils with different tracks.

the 3 strip track and least in the 12 strip. Averaging over all measurements, the 12 strip has 90% of the dM/dx with no track, the 6 strip 87% and the 3 strip 83%. Since drive force is proportional to dM/dx, this means that with a 3 strip track, the drive force will only be 83% of the values calculated without considering the effect of the track. The observed reduction in dM/dx with wider strips agrees with the theory presented in section 3.2 that predicts larger eddy currents with wider tracks.

20 KHz was the only frequency used for these tests. This frequency has a skin depth only one-fifth the thickness of the guide strips, and therefore gives the high speed limit of the effect of the guideway on the drive force.

3.6 Drag Force Calculations

In order to calculate drag force profiles for the different tracks, AC resistance was measured as a function of bucket position. However, due to difficulties with the measurement apparatus, sufficient accuracy could not be obtained to notice the differences of AC resistance with position.

Special care must be taken to measure the AC resistance of highly inductive resistors with bridge circuits. The opposing arm to the unknown must be balanced with a comparable reactance. For this experiment a capacitor was connected to one arm of the bridge (as suggested in the manual), but even with

TABLE 5

DRAG FORCE MEASUREMENTS

	Bucket Centered in Track		
TRACK	L(μH)	R(mΩ)	V_{F_d}/I_o^2 (W/amp^2)
3 strip	324.5	810	6.61×10^{-5}
6 strip	326.1	800	6.51×10^{-5}
12 strip	327.0	800	6.55×10^{-5}

this addition only two-digit accuracy could be reached, at the sensitivity limit of the null detecter. They are presented in Table 5. The calculations of drag power used Eq. (3.6). The result is that all tracks have about the same drag power. This is opposed to the simple theory of variation of eddy currents with strip width (Section 3.2) which predicts that the 12 strip track should have less than one-half of the drag power of the 3 strip track.

Due to this lack of agreement with a very compelling theory, combined with the lack of confidence with the experimental results, the above results are not believed to be correct.

The experiment was not repeated due to limitations of time. Measurements of drag power have been completed successfully by other experimenters,[8] so there is no fundamental problem with such AC resistance measurements. The problems with the models reported on in this paper were probably due to contact resistance in the connections, which become dominant when measuring low resistances.

3.7 Conclusions

It was shown in Section 3.2 that dividing a given aluminum area into smaller regions increases effective resistivity and therefore decreases eddy currents. This means that guidance

force drag and reduction of drive force will all increase as the number of strips decreases assuming that we use the same total amount of aluminum.

Figure 21 shows the variation of guidance force with number of strips measured with the impedance models. The value given is the average over angle of restoring force just before contact. This variation is explained by the theory presented in Section 3.2, which predicts that the eddy currents and thus the force will vary as $1/\sqrt{n}$, where n is the number of strips.

This same theory also predicts the variation of drag with number of strips. If a sheet of aluminum is divided into n pieces (see Fig. 10) and I and R are the eddy current and resistance of each piece, then I and R vary as $1/\sqrt{n}$ and total drag power varies as

$$P_t = nI^2R \sim \frac{1}{\sqrt{n}} \tag{3.17}$$

Thus, like restoring force, drag power varies inversely as the square root of number of strips. A plot of this variation is shown in Fig. 22.

Finally, the same theory predicts a greater reduction of drive force with fewer strips. This is confirmed by the experimental results shown in Fig. 23.

Although average guidance force increases with wider strips, the force varies more with angle. Figure 24 is a plot of the percentage difference between force at a gap and force at a strip for tracks with different numbers of strips. These are experimental results from impedance modeling, with all tracks using the same amount of aluminum.

We can reduce this angular variation by using more aluminum (i.e., by making some number of wider strips). This will produce two undersirable effects however:

1. It will increase drag
2. It will increase shielding by the track of the drive force.

The effect of using tracks with different amounts of aluminum was not investigated with the impedance models.

To summarize, the track designer must make the following trade-off:

- the guide strips must be wide enough to produce enough restoring force to prohibit contact. However, they should be no wider, since this will produce greater drag and reduction of drive force.
- the gaps between the strips must be made small enough to produce guidance forces at the gap strong enough to prohibit contact. However, the gaps should be no smaller, since this will use more aluminum which implies greater drag and reduction of drive force, and also greater overall mass of the mass driver.

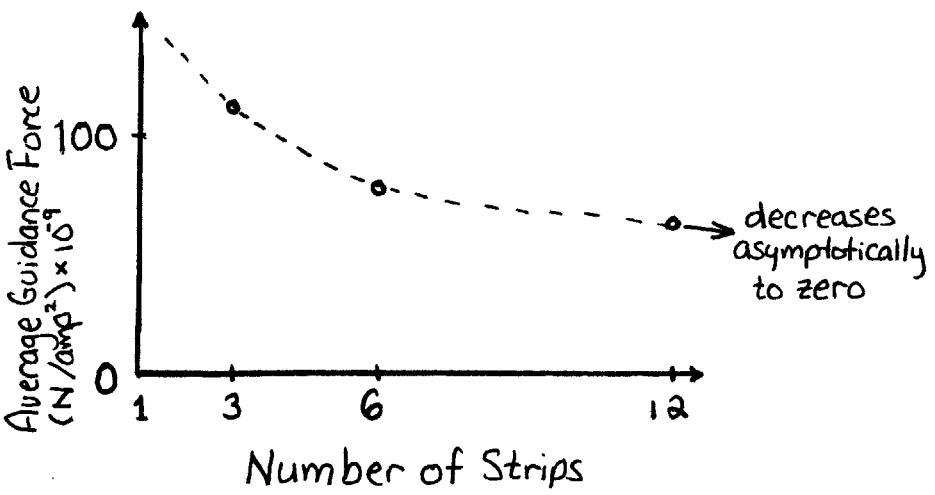

Figure 21. Measured variation of guidance force with number of strips.

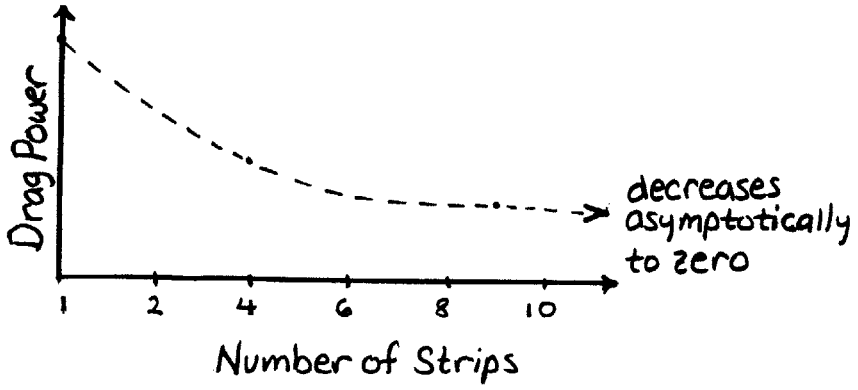

Figure 22. Theoretical calculation of variation of drag with number of strips.

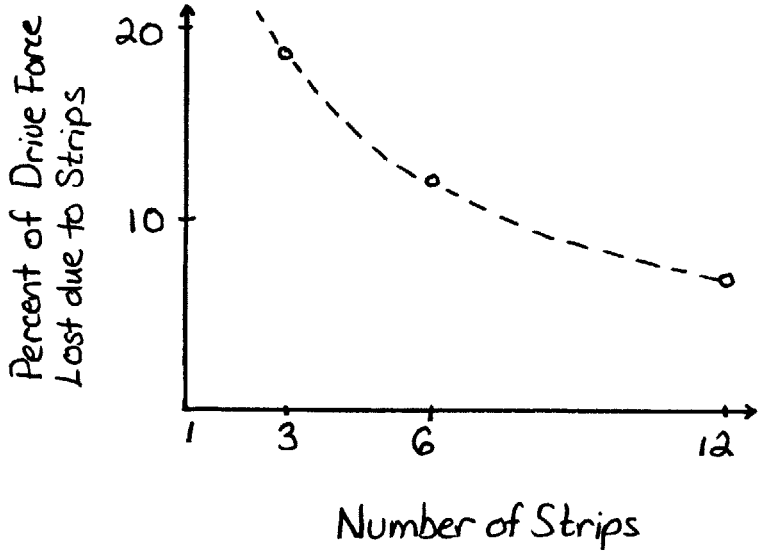

Figure 23. Measured percent reduction of dM/dx with number of strips.

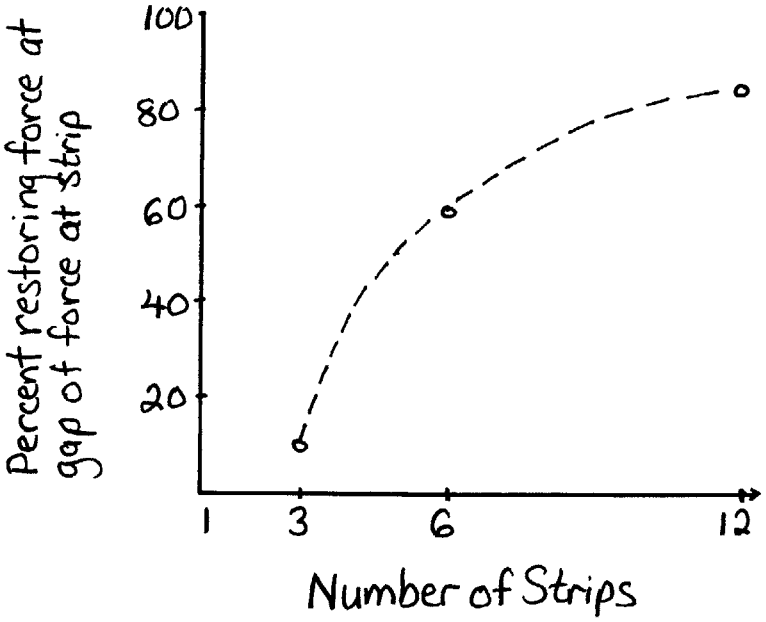

Figure 24. Measured percent difference between force at a gap and force at a strip with number of strips.

APPENDIX A: OTHER RELEVENT PUBLICATIONS ON MASS DRIVERS

A summary of research up to the Spring of 1977 can be found in four papers presented at the May 1977 Princeton Conference on Space Manufacturing Facilities. The proceedings have been published as a bound volume by the AIAA. The relevent papers are:

> "Mass Driver Reaction Engine as Shuttle Upper Stage," by G.K. O'Neill.
>
> "Basic Coaxial Mass Driver Reference Design," by Henry Kolm.
>
> "Mass Driver Theory and History," by Frank Chilton.
>
> "Mass Driver Construction and Testing," by Kevin Fine.

Later work completed during a NASA/AMES summer study during the summer of 1977 is presented in three papers to be published as a NASA Special Publication. This work is summarized in a brief but very valuble paper:

> "Mass Driver for Lunar Transport and as a Reaction Engine," by G.K. O'Neill and Henry Kolm.

This paper was presented at the XXVIIIth Congress of the International Astronautical Federation in September 1977 and was published in the Journal of the Astronautical Sciences, Vol. XXV, No. 4. Other articles that may be useful are:

"Space Colonies and Energy Supply to the Earth," by G.K. O'Neill in Science, 5 December 1975, Vol. 190.

"The Colonization of Space," by G.K. O'Neill in Physics Today, Vol. 27, September 1974.

"An Electromagnetic "Slingshot' for Space Propulsion," by Henry Kolm in Technology Review, Vol. 79, No. 7, June 1977.

"Engineering a Space Manufacturing Center," by G.K. O'Neill in Astronautics and Aeronautics, October 1976.

Finally, the most up to date and useful article that includes some interesting graphs is:

"The Low (Profile) Road to Space Manufacturing," by G.K. O'Neill in Astronautics and Aeronautics, March 1978.

REFERENCES

1. Clarke, A.C., "Electromagnetic Launching as a Major Contribution to Spaceflight," JBIS, Vol. 9, No. 6, November 1950.

2. O'Neill, G.K., "The Colonization of Space," Physics Today, Vol. 27, No. 9, September 1974, pp. 32-40.

3. O'Neill, G.K., Kolm, H.H., "Mass Driver for Lunar Transport and as a Reaction Engine," International Astronautical Federation (I.A.F.) XXVIIIth Congress, September 1977.

4. Kolm, H. , "Basic Coaxial Mass Driver Reference Design," AIAA Paper 77-534.

5. Fine, K., "Basic Coaxial Mass Driver Construction and Testing," AIAA Paper 77-535.

6. Arnold, W., Bowen, S. Fine, K., Kaplan, D., Kolm, H., Kolm, M., Newman, J., O'Neill, G.K., and Snow, W., "Mass Drivers III: Engineering," (in preparation as chapter in NASA Special Publication).

7. Wong, J.Y., Mulhall, B.E., Rhodes, R.G., "The Impedance Modelling Technique for Investigating the Characteristics of Electrodynamic Levitation Systems," J. Phys. D: Appl. Phys., Vol. 8, 1975, pp. 1948-55.

8. Gunderjahn, C.A., Wipf, S.L., Fink, H.J., Boom, R.W., MacKenzie, K.E., Williams, D., Downey, T., "Magnetic Suspension for High Speed Rockets by Superconducting Magnets," J. Appl. Phys., Vol. 40, No. 5, 1969, pp. 2133-40.

9. Grover, F.W., Inductance Calculations, Dover, N.Y., 1946.